Magnesium as promoter of the CO_2 methanation on Ni-based USY zeolites

Maria C. Bacariza[a], Inês Graça[b], Suse S. Bebiano[c], José M. Lopes[a], Carlos Henriques[a,*]

[a]Centro de Química Estrutural, Instituto Superior Técnico, Universidade de Lisboa, Av. Rovisco Pais, 1049-001 Lisboa, Portugal

[b]Department of Chemical Engineering, Imperial College London, London SW7 2AZ, United Kingdom

[c]Technology and Innovation Centre, University of Strathclyde, 99 George Street, Glasgow, G1 1RD Level 6

*Corresponding author: carlos.henriques@tecnico.ulisboa.pt

Abstract

CO_2 methanation was studied over Ni-Mg-USY zeolite catalysts. Mg was added by incipient wetness impregnation and ion-exchange. Whatever the Mg incorporation method used, Mg is able to improve the performances of the Ni-zeolite catalysts. Magnesium impregnation at lower contents (below 2.5%) over a 5%Ni/zeolite leads to an enhancement of the CO_2 conversion into methane of 15% at 350-450ºC, probably due to the induced increase of the Ni particles dispersion, as well as to the possible activation of CO_2 on the defects present on the MgO surface. At higher Mg contents, the stronger interaction between Ni and Mg oxides, leading to the formation of NiO-MgO solid solutions, seem to reduce the reducibility of the Ni species, decreasing the amount of nickel active sites available, and, so, the catalytic performances. Furthermore, important improvements of the catalytic performances (CO_2 conversion and CH_4 selectivity increased around 20% at 350-450ºC) were also found for the Mg-exchanged 5%Ni/zeolite. The results are comparable to those obtained by impregnation, but lower Mg contents are required. The enhanced activation of CO_2 on Mg^{2+}, the more dispersed Ni particles on the support, as well as the enhanced Ni reducibility when compared to the impregnated catalysts, can explain the observed results. The beneficial effect of the Mg addition both by impregnation and ion-exchange was also observed for samples containing higher amounts of Ni, the best sample remaining stable after 10h under reaction conditions. Thus, Mg could be an interesting promoter for the CO_2 methanation over Ni-zeolite catalysts.

Keywords: Magnesium, zeolites, nickel, CO_2 methanation, compensating cations

1. Introduction

The use of CO_2 as feedstock for the production of chemicals and fuels has been focus of several investigations in the last years [1,2]. In fact, carbon dioxide has been already used in several industrial processes, mainly those involving reductions, additions, coupling and acid-base reactions. The synthesis of urea (for nitrogen fertilizers and plastics), salicylic acid (pharmaceutical ingredient) and polycarbonates (for plastics) are examples of commercial processes in which CO_2 is already used as raw material [3].

Nevertheless, the conversion of CO_2 into fuels could constitute a more effective and sustainable alternative to mitigate CO_2 emissions, since, besides decreasing the amount of CO_2 released to the atmosphere, it could lead to a reduction in the consumption of carbon-based fossil resources for energy generation [3]. Between all the possibilities to convert CO_2 into fuels, the most investigated area has been the CO_2 hydrogenation into oxygenates and hydrocarbons, which has as main drawback the fact that hydrogen is required. This can be produced from renewable sources of energy, like solar energy or wind, via water electrolysis [4].

CO_2 methanation has been reported as a process with high thermodynamic conversion and selectivity at temperatures below 770ºC [5]. Several catalytic systems have been investigated for the conversion of CO_2 into methane [3,6], being SiO_2, Al_2O_3, CeO_2, ZrO_2, Ce/Zr, zeolites and mesoporous materials used as supports. The main metals used are nickel and noble metals such as Rh and Ru. It was also reported in the literature [7–14] the beneficial effects of the presence of MgO on catalysts used in CO_2 or CO methanation, due to the formation of highly dispersed active metal particles [9,10,15]. In addition, it was proposed a mechanism in which CO_2 is preferentially adsorbed on MgO and reduced metals are needed for the supply of H atoms [7,8]. Compensating cations, such as K^+, Cs^+ or even Mg^{2+}, have also been reported as promoters for CO_2 adsorption on different types of zeolites [16–21], being the larger metal alkali cations able to suppress the process of metal agglomeration on Ni based zeolites [22].

In our previous studies, it was reported the suitability of Ni-based zeolites for the conversion of CO_2 into CH_4, as well as the effects of some changes in the preparation method, the effect of cerium incorporation and some highlights about the mechanism of the reaction and the activation sites for CO_2 methanation in an USY zeolite support [23–25]. In the present study, the effect of magnesium incorporation on Ni-based USY zeolites will be evaluated. This is a new topic of research since no works can be found in the literature

dealing with Ni-Mg-zeolite systems as catalysts for this reaction. Magnesium addition to the Ni/USY was carried out both by incipient wetness impregnation and by ion-exchange, and different magnesium contents were investigated. The samples were characterised by ICP elemental analysis, X-Ray diffraction (XRD), N_2 adsorption, hydrogen temperature programmed reduction (H_2-TPR), transmission electron microscopy (TEM) and temperature programmed desorption of CO_2 (CO_2-TPD).

2. Experimental section

2.1.Catalysts preparation

Zeolite-based samples were prepared using an Ultra-Stable Y zeolite (USY) supplied by Grace Davison as support. The main physicochemical and textural properties of this material are summarised in Table 1. All samples prepared in the present study, as well as the preparation conditions and the labels used according to ICP analysis results, are shown in

Table **2**.

Several samples were used as reference catalysts. These samples were MgO provided by Merck with 99.9% purity, NiO provided by Sigma Aldrich with 99.99% purity, one sample of Mg impregnated over USY zeolite and one sample of Ni impregnated over the commercial MgO.

Samples of Mg impregnated over 4.8%Ni/USY were prepared by incipient wetness impregnation and using magnesium nitrate hexahydrate ($Mg(NO_3)_2 \cdot 6H_2O$, Sigma-Aldrich, 99.7%) as precursor salt. An aqueous solution of Mg salt with a water volume close to that of the zeolite pores was added drop by drop to the Ni/USY sample, being the suspension kept under stirring. After that, samples were dried overnight at 80ºC and, finally, calcined at 500ºC under air flow. Another Ni-Mg sample was prepared by impregnating 10%Mg on 14%Ni/USY following the same procedure detailed before.

Finally, samples with Mg as compensating cation were prepared following the procedure illustrated in Figure 1. As it can be seen, firstly, the acidic form of the USY zeolite was obtained by ion-exchanging a certain mass of zeolite with a NH_4NO_3 solution (Volume of solution per gram of zeolite = 4 ml/g), keeping it under stirring and reflux during 4 hours at 100ºC. After that, the samples were filtered, dried overnight and calcined at 500ºC under air flow. Two parts of this sample were impregnated with ~5 and ~15%Ni and calcined at 500ºC by following the same procedure described previously, in order to use these samples as

reference for this chapter. Later, the same H-USY support was again ion-exchanged with a $Mg(NO_3)_2$ solution with the conditions specified in Figure 1. Two preparations were carried out in order to obtain different exchange degrees: a single ion-exchange and three consecutive ion-exchanges, both followed by drying of the samples at 100ºC overnight and calcination at 500ºC. Finally, and following the procedure of impregnation described above, ~5 and ~15%Ni were incorporated in the samples using nickel nitrate hexahydrate ($Ni(NO_3)_2 \cdot 6H_2O$, Sigma-Aldrich, >99%) as precursor salt.

2.2.Catalysts characterisation

Catalysts were characterised by ICP elemental analysis, X-Ray diffraction (XRD), N_2 adsorption, hydrogen temperature programmed reduction (H_2-TPR), transmission electron microscopy (TEM) and temperature programmed desorption of CO_2 (CO_2-TPD).

Catalysts elemental analysis was performed by inductively coupled plasma (ICP) in the *Laboratório Central de Análises* (*Universidade de Aveiro*, Portugal), in order to determine the composition of the prepared catalysts.

XRD patterns were obtained in a Bruker AXS Advance D8 diffractometer, using Cu Kα radiation and operating at 40 kV and 40 mA. The scanning range was set from 5° to 80° (2θ), with a step size of 0.03º/2s. This technique was used to verify if the introduction of Mg leads to damages in the zeolite structure and also to detect the presence of Ni, Mg and Ni-Mg species in the samples.

N_2 adsorption measurements were carried out at -196ºC on a Micrometrics ASAP 2010 apparatus. Before adsorption, zeolite samples were degassed under vacuum at 90ºC for 1h and then at 350ºC for at least 4h. The total pore volume (V_{total}) was calculated from the adsorbed volume of nitrogen for a relative pressure P/P_0 of 0.97, whereas the micropore volume (V_{micro}) and the external surface area (S_{ext}) were determined using the t-plot method. The mesopore volume (V_{meso}) was given by the difference $V_{total} - V_{micro}$.

H_2-TPR experiments were performed in a Micromeritics AutoChem II equipment, where the catalysts were, firstly, pre-treated at 250°C under argon flow and then cooled down to the room temperature. After that, the reduction of the catalysts was carried out over a 5%H_2/Argon flow, rising the temperature from the room temperature to 900°C. The hydrogen

consumed was monitored by a TCD detector. This technique was used for the evaluation of Ni species reducibility in the different samples, as well as for the detection of Ni-Mg interactions.

TEM analysis was performed for several reduced samples (470ºC) at *Université Pierre et Marie Curie* (Paris, France) using a HRTEM 2010 JEOL LaB6 microscope (200kV).

CO_2-TPD was carried out in a fixed-bed flow reactor. The catalyst (m ~ 200 mg) was reduced in-situ at 470˚C for 1 h under 80%H_2/N_2 flow, then flushed under N_2 and cooled down to 50˚C under the same atmosphere. Then, the gas mixture was switched to pure CO_2 for 30 min until the adsorption equilibrium was reached. After that, the excess adsorptive gas was purged with an N_2 flow for 30 min, the catalyst was heated up to 700˚C at a rate of 10˚C min^{-1} in the N_2 flow, and desorbed species were analysed using a CO_x Siemens Ultramat 23 infrared detector.

2.3.Catalytic tests

The catalytic tests were carried out in a Pyrex reactor, under atmospheric pressure. The reactor was heated in a TermoLab electric oven, using a temperature controller, and a thermocouple was placed inside the reactor close to the catalytic bed, in order to follow the variation of the temperature of the sample during the tests. The gases were supplied by Air Liquid with purities above 99.9990%.

Before the catalytic tests, samples were pre-reduced at 470ºC for 1h, except for one of the tests where the reduction temperature was increased to 700ºC, in order to increase the amount of Ni species reduced and verify the effects on the catalytic performances. A flux of 80%H_2/N_2 was used, with a total gas flow of 250 mL min^{-1}. Reactivity tests were accomplished using a feed constituted by H_2, CO_2 and N_2 at a molar ratio of 36:9:10 and a total flow of 250 mL min^{-1}, being the flows controlled by mass Brooks flowmeters. The mass of catalyst used was the same in all the catalytic tests in order to keep the gas hourly space velocity (GHSV) approximately constant (43000 h^{-1}). The reaction was performed at temperatures ranging from 250 to 450ºC. A long-term test was also carried out for a selected sample during 10h at 400ºC.

The amounts of CO and CO_2 produced were analysed using a CO_x Siemens Ultramat 23 infrared detector. In addition, the amount of CH_4 was measured in a 5890 HP Series II Gas

Chromatograph (GC), equipped with a Poraplot Q capillary column (25m, helium as carrier gas) and a flame ionization detector (FID). At each temperature, after the stabilization of the catalytic system (steady-state), three measures of CO, CO_2 and CH_4 were taken and an average value was calculated. In all cases, CO and CH_4 were the only products detected from CO_2 hydrogenation.

3. Results and discussion

3.1. Effect of Mg impregnation on a 5%Ni/USY zeolite

Impregnation is a common method applied in the preparation of catalysts used in the CO_2 methanation reaction [3,26]. As a result, impregnation was chosen for the preparation of several Mg-Ni/USY catalysts with Mg contents from 0.9 to 13.0%. Mg was incorporated over a previously reported [23] 4.8%Ni/USY sample.

3.1.1. Catalysts characterization

XRD diffractograms for the different Ni-Mg samples, as well as for the USY zeolite and the 4.8%Ni/USY, can be seen in Figure 2. The range between 41.5 and 45.5º was detailed, since it can be used for the detection of the presence of $Ni_xMg_{(1-x)}O_2$ mixed oxides. As it can be observed in the complete diffractograms, catalysts with 0.9 and 2.5%Mg present almost no differences when compared to the reference materials (4.8%Ni/USY and USY). However, in the case of the catalyst with 5.6%Mg, a partial decrease of the zeolite characteristic peaks intensity can be seen, indicating a partial loss of the sample crystallinity. Finally, the sample containing 13.0%Mg presents a much more evident decrease in the peaks intensity, as well as the appearance of an amorphous band from 15 to 40º, which shows that an important damage of the zeolite structure has occurred. Moreover, it is known that $Ni_xMg_{(1-x)}O_2$ solid solutions can be formed in the presence of these metals. It was shown in the literature [10,27–34] that the detection of these species can be verified by following the evolution of the NiO and MgO diffraction peaks with the Mg addition. Indeed, analysing the diffractograms in the 41.5-45.5º range, single NiO and MgO peaks at ~ 43.5º and 42.9º respectively can be observed at low Mg contents, whereas with the increase of the Mg addition an unique broad peak starts being formed, centred at about 43.1º for the sample with the highest Mg content. This could be attributed to the presence of $MgNiO_2$ species, and might indicate the formation of $Ni_xMg_{(1-x)}O_2$ solid solutions. In addition, another broad peak around 45.1º can be observed for the sample with 13.0%Mg, which could be related to the presence of $NiAl_2O_4$ and/or $MgAl_2O_4$ in the samples, according to the literature [10,27–35].

However, the identification of these species should be confirmed by other characterization technique, such as H_2-TPR.

In order to characterize the main catalysts in terms of textural properties, N_2 adsorption experiments were carried out (Table 3). As it can be noticed, the samples with lower Mg content do not present significant differences, when compared to the 4.8%Ni/USY or USY zeolites. However, in the case of the sample with the highest amount of impregnated Mg, a drastic decrease of the microporous volume can be observed. This important decrease might be attributed, according to the XRD results, to the structural damage observed for this sample. In addition, the formation of large particles of $Ni_xMg_{(1-x)}O_2$ solid solutions detected by XRD could also be responsible for the blockage and/or destruction of some zeolite micropores.

H_2-TPR profiles for the samples with Mg impregnated over a Ni/USY, as well as for the reference materials, can be found in Figure 3. Starting by the analysis of the reduction profiles obtained for the reference materials, in the 7.0%Mg/USY (profile b), where Mg was impregnated in the USY support, a more intense peak can be observed at 600ºC, as in the case of MgO (profile a), and two smaller peaks can be seen at 450 and 760ºC. The lack of studies on Mg impregnated over zeolites presenting H_2-TPR profiles does not allow properly attributing these peaks, but they might be related to the reduction of MgO species interacting in different ways/strengths with the zeolite. Furthermore, for the sample prepared by impregnating 5.0%Ni over MgO (profile e), mainly four peaks can be observed at 350, 470, 600 and 800ºC, the more intense being the one at 350ºC. In this case, the peak at 350ºC can be assigned to the reduction of dispersed NiO particles with lower interaction with the support [31,36], resulting the others from different interactions between Ni and MgO, leading to the formation of $NiMgO_2$ species, as it will be discussed later in this work. When Ni is impregnated over the USY zeolite (profile d), peaks referred to NiO (profile c) and Ni^{2+} species located both on the surface and on the internal cavities of the zeolite could be detected (390, 485, 690 and 740ºC). Concerning the Mg-Ni samples (profiles f to i), mainly 5 different reduction peaks (α, β, γ, δ and ε) can be observed. Peaks identified as α and β, mainly present in the samples with lower Mg content and in the 4.8%Ni/USY zeolite, could be attributed to the reduction of free NiO species with no interactions with both MgO and the zeolite [31]. In addition, peaks γ, δ and ε, more intense in the samples with higher % of Mg, could be related to the reduction of Ni species interacting with MgO and with the support. In fact, it was suggested [31] that peaks around 600ºC could be ascribed to the reduction of surface

NiO with a medium interaction with MgO, and peaks about 700 and 800ºC could result from the reduction of NiO on the outermost layer of $Ni_xMg_{(1-x)}O_2$ solid solution. In another study using Ni-Mg/SiO_2 catalysts [10], authors attributed peaks from 530 to 630ºC to the reduction of surface, subsurface and bulk phase Ni ions in the outer-like layers of MgO, and peaks around 730ºC to the reduction of Ni ions on subsurface layers of MgO lattice. Other authors [27,37] suggested that peaks at ~ 800ºC can be ascribed to the reduction of nickel aluminate phase, detected, as previously mentioned, in the powder XRD diffractograms at $2\theta = 45.1º$. These peaks reported in the literature (~ 600, ~700 and ~800ºC) can be clearly found in the samples with high %Mg (profiles h and i, mainly), indicating the existence of $Ni_xMg_{(1-x)}O_2$ species in these samples, as indicated previously. Moreover, the shift detected in the temperatures for the maximum of the identified peaks (α, β, γ, δ and ε), which increase with the increase of the Mg content, has been already reported in several works [10,27,38–40]. This is related to the presence of stronger interactions between Ni and Mg species because of the stabilisation of Ni species in periclase Mg(Al)O, by the formation of solid solutions as Mg(Ni,Al)O, this effect being more important at higher Mg contents. In addition, the verified decrease of Ni reducibility at low temperatures was suggested in the literature as beneficial for some reactions [39], since, when this Ni strongly interacting with MgO is reduced, the Ni^0 particles will not be fully exposed on the surface and, as a result, sintering processes will be prevented.

TEM micrographs of the samples containing Ni and Ni-Mg and pre-reduced at 470ºC are shown in Figure 4. As it can be seen, when present in smaller amounts, Mg improves the dispersion of Ni, leading to lower average Ni^0 particles size (from 19 nm in 4.8%Ni/USY to 12 nm in 0.9%Mg 4.3%Ni/USY and 11 nm in 2.5%Mg 3.7%Ni/USY). This effect of Mg on the Ni^0 particles size has been already reported in the literature [9,10,15]. For the sample with the highest % of Mg, no clear Ni^0 particles could be found. This could be a result of the strong structural damage of the zeolite and also due to the formation of NiO-MgO solid solutions. On the other hand, when using MgO directly as support for the Ni particles (4.8%Ni/MgO), the detection of a significant amount Ni^0 species in the TEM micrographs (not shown) was difficult because of the lower dispersion, and an average Ni^0 particle size between 25 and 35 nm was determined. This indicates that the Ni^0 particles are smaller and better dispersed when supported on the zeolite in presence of a small % of Mg.

In order to further understand the effect of the MgO on the Ni-Mg/USY catalysts activity, the CO_2-TPD profiles for the USY zeolite used as support, the 4.8%Ni/USY sample and a catalyst containing impregnated Mg were measured (Figure 5). As it can be observed,

both USY and Ni/USY catalysts presented practically no CO_2 desorption peaks. However, in the case of the impregnation with 2.5%Mg, an important CO_2 desorption band can be observed from 80 to 435ºC, with maximum at 170ºC. This clearly shows that the interaction between CO_2 and the catalysts is higher in the presence of Mg, which might be associated to the capacity of MgO to adsorb CO_2. This can be a relevant additional step of CO_2 activation towards methanation. In the literature [8], similar peaks at temperatures below 450ºC were reported for Pd-MgO/SiO_2 systems with low amounts of Mg (0-3.6%). The authors considered that small amounts of MgO could dramatically improve the CO_2 adsorption and, consequently, the CO_2 conversion, due to the lower stability of the MgO formed at low Mg contents and to the likely presence of defective surfaces with vertices, steps or kinks where low-coordinated or protruded oxygen atoms could be found. Thus, these oxygen atoms could bind, and, as a result, activate the very stable CO_2 molecule through the formation of carbonate species.

3.1.2 Evaluation of the catalytic performances

The catalytic results obtained for the Mg-Ni samples are shown in Figure 6. In general, it is possible to see that the impregnated zeolite catalysts containing Mg present better CO_2 conversions and CH_4 selectivity than the 4.8%Ni/USY and 4.8%Ni/MgO catalysts, which reveals the beneficial effect of adding Mg to the zeolite-supported catalysts. Nevertheless, performance increases up to 2.5% of Mg, decreasing at higher Mg contents. In fact, the impregnation of 2.5% Mg on the 4.8%Ni/USY catalyst can lead to an enhancement of 15% in the CO_2 conversion and 20% in CH_4 selectivity. This enhancement in the catalytic performances is also important for the catalyst containing 0.9%Mg. This effect could be attributed, as previously referred in the discussion and interpretation of the CO_2-TPD and TEM, to the activation of CO_2 in the less-stable MgO species present at low Mg amounts, as well as to the lower Ni^0 average particle size and better metal dispersion in the catalysts with lower Mg content. This enhancement of the Ni dispersion is very relevant, since, as referred in the literature [7,8], Ni^0 sites are responsible for the dissociation of H_2, supplying the H atoms for the CO_2 hydrogenation. On the other hand, samples with 5.6 and 13.0%Mg do not lead to so important benefits in terms of catalytic performances, probably due to the lower Ni reducibility in these samples and also to the partial damage of the zeolite structure.

The promoter effect of Mg is the opposite of the observed in our previous work dealing with the effect of cerium incorporation over Ni/USY catalysts [23], where it was

verified that the higher the amount of Ce, the better the catalytic performances achieved. These different effects could be due to the strong interaction of NiO with MgO, mainly found at higher %Mg. These interactions avoid the reduction of Ni species at temperatures below the pre-reduction one (470ºC), drastically decreasing the amount of Ni^0 for the activation of H_2, and could lead to important damages in the zeolite structure. In the case of CeO_2, however, the presence of higher amounts favoured the dispersion of Ni and increased its reducibility at lower temperatures. By comparing the results obtained for a catalyst with 15%Ce 5%Ni/USY with the 2.5%Mg 3.7%Ni/USY, it could be observed that the performances of the sample containing Ce are higher than those of the Mg sample (CO_2 conversions of 52 and 39% and CH_4 selectivity of 86 and 74% at 400ºC respectively), but not so different considering the amounts of Ce and Mg on the catalysts.

3.2. Effect of Mg as compensation cation on a 5%Ni/USY zeolite

The effect of incorporating Mg on the USY zeolite by ion-exchange prior to the impregnation with Ni was also studied. With this purpose, and as previously reported, two samples were prepared in order to achieve different ion-exchange degrees in the zeolite structure. Two supports with estimated Mg^{2+} exchange degrees of ~30 and ~60% were obtained and impregnated with similar Ni contents.

3.2.1. Catalysts characterization

XRD diffractograms for the Ni-containing Mg-exchanged samples did not reveal any structural modifications, when compared to those of the reference materials (Figure 7). Regarding the detailed results from 41.5 to 45.5º, no important peaks attributed to MgO and/or solid solutions between NiO and MgO are observed, suggesting that the main part of Mg is present in the samples as Mg^{2+}, compensating the negative charges of the zeolite structure. However, a slight shift towards lower 2θ can be observed for the NiO peak, which might indicate the presence of a small fraction of Mg partially interacting with Ni, maybe in the form of $Ni_xMg_{(1-x)}O_2$ species.

By N_2 adsorption results (Table 3), it can be noticed that the ion-exchange of Mg followed by the impregnation of nickel leads to some changes in terms of textural properties. Indeed, a slight increase is noticed in the microporous volume, whereas an important increase is observed in the mesoporous volume. In addition, an increase of the surface area with the Mg ion-exchange can also be verified. Therefore, it appears that the ion-exchange with Mg^{2+}

leads to an increase of the porosity, which could facilitate the access of the reagents to the internal porous of the zeolite. In order to understand the improved textural properties in these samples, ICP analysis was performed, to determine the %Al and %Si on the zeolite samples. It was verified that there is a relevant increase in the global Si/Al ratio for these samples (to 3.6/3.7), which was due to a decrease of the % of Al on the samples. This could suggest that some dealumination could have occurred during the ion-exchange processes, perhaps mainly through the lixiviation of the EFAL species present in the initial USY sample. Indeed, the Mg-exchanged zeolites present a Si/Al ratio that is similar to the framework Si/Al of the initial USY sample. The removal of the EFAL species from the zeolite structure could have led to higher volumes and external surface areas.

Furthermore, and in order to study the reducibility of the different ion-exchanged Mg samples, H_2-TPR profiles are shown in Figure 8. It can be noticed that, when comparing these samples with the 4.8%Ni/USY, additional reduction peaks can be observed at 270, 527 and 827ºC. The first peak at 270ºC is close to the observed in Figure 3 for the reduction profile of 5.0%Ni/MgO and ascribed to the reduction of Ni species weakly interacting with MgO. The peak at 527ºC is close to the observed at 500ºC on the catalyst containing only Ni, so it could be attributed to the reduction of a great fraction of NiO species in the supercages of the USY zeolite. The reduction peak at 827ºC could be assigned to the reduction of NiO species on the outermost layer of $Ni_xMg_{(1-x)}O_2$ solid solution. Thus, these observations indicate that a fraction of the ion-exchanged Mg will be present in a mixed oxide with NiO and not as compensating cation. However, it is important to refer that the H_2-TPR profiles of the Mg exchanged USY supports before the introduction of Ni (not presented in the Figure) did not reveal any reduction peaks, suggesting that the fraction of Mg present as MgO, NiO-MgO or $MgAl_2O_4$ species in the sample is not relevant.

TEM micrographs displayed in Figure 9 show that the presence of Mg as compensating cation on the zeolite structure favours Ni dispersion, similarly to what happens for the samples with impregnated Mg at lower contents. Once again, from the analysis of the images, the average particle size for Ni^0 was calculated. For the samples with 0.7% and 1.4% exchanged-Mg, Ni^0 particles are about 11 nm and 13 nm, respectively, being effectively smaller than the Ni^0 particles on the 4.8%Ni/USY (19 nm). This indicates that Mg ion-exchanged leads to an enhancement of the Ni dispersion with a decrease in the average particle size. Nevertheless, no significant differences in terms of Ni^0 particles size could be observed by incorporating Mg through ion-exchange or impregnation.

3.2.2. Evaluation of the catalytic performances

The performances obtained for the 5%Ni Mg-exchanged zeolite catalysts are shown in Figure 10A. As it can be seen, the presence of exchanged-Mg on the USY structure also leads to an enhancement of the CO_2 conversion and CH_4 selectivity, as observed before for the impregnated catalysts. The performance improvement for the sample containing 1.4% of exchanged Mg^{2+} can be indeed compared with that obtained for the 2.5%Mg impregnated catalyst, even if the amount of exchanged-Mg is not as high (8.9 mol of $CO_{2converted} \cdot h^{-1} \cdot g^{-1}$ Mg and 6.6 mol of $CH_{4produced} \cdot h^{-1} \cdot g^{-1}$ Mg for the impregnated sample and 15.9 mol of $CO_{2converted} \cdot h^{-1} \cdot g^{-1}$ Mg and 12 mol of $CH_{4produced} \cdot h^{-1} \cdot g^{-1}$ Mg for the ion-exchanged sample). This could be attributed to the activation of the CO_2 in the Mg^{2+} acting as compensating cation, as suggested in our previous work [25]. Indeed, CO_2 adsorption in zeolites was in fact reported to be strongly affected by the type and nature of the compensation cation [16–18,20,42]. The basicity of the Mg^{2+} ion-exchanged sample leading to the best catalytic performances was also verified by CO_2-TPD in the present study (Figure 10B), the results being compared with the obtained for a Mg impregnated sample. From the analysis of the profiles one can conclude that the basicity of the samples is not directly responsible for the differences on the performances of these samples. Indeed, the Mg impregnated sample presents higher basicity both in terms of strength and number of centers. Thus, the important effect of Mg^{2+} in the decrease of the Ni^0 particles average size, the higher reducibility of Ni species and the interaction with CO_2 molecules could be considered as responsible for the better catalytic performances achieved.

3.3. Samples containing 15% of Ni

In order to verify if the same enhancement of the catalytic performance could also be obtained for the Mg-containing samples with higher Ni contents, several preparations with ~15%Ni were carried out for both Mg impregnated and Mg as compensating cation on the zeolite.

3.3.1. Mg impregnation

A 14%Ni/USY catalyst already reported in our former studies [23,24] was impregnated with Mg. The choice of the %Mg to be incorporated was done by analysing the Ni/(Mg+Ni) ratio leading to the best catalytic performances in samples with lower Ni contents (Table 4).

As a ratio Ni/(Ni+Mg) of 0.6 was found to be the optimal in terms of CO_2 conversions and methane selectivity, a sample with 9%Mg 13%Ni/USY was prepared by impregnating Mg over the 14%Ni/USY zeolite. This sample was characterized by XRD and H_2-TPR (Figure 11). XRD diffractograms (Figure 11A) show that there were no structural damages to the zeolite structure after both Ni and Mg additions. Furthermore, it can be noticed the presence of NiO and MgO peaks, as well as the correspondent mixed oxides: NiO-MgO, $NiAl_2O_4$ and $MgAl_2O_4$. In terms of reduction profiles (Figure 11B), an important decrease in the reducibility of Ni species at temperatures below the pre-reduction can be observed. The shift to higher temperatures of the reduction peaks between 400 and 800ºC for Ni species observed in the Ni/USY samples indicates the establishment of strong interactions between Ni, Mg and the zeolite support, as observed in the case of the samples with lower Ni content. In the catalytic performances (Figure 12A), no important effects of the Mg incorporation were observed when comparing the results obtained for the samples with and without Mg. However, it is necessary to take into account that these samples were pre-reduced at 470ºC. Therefore, and as the reduction of Ni species was observed to occur at higher temperatures for these Mg-Ni samples, another catalytic test was carried out after reduction of the Mg-Ni zeolite at 700ºC. In our previous studies[24], the results for the 14%Ni/USY sample were reported not to be affected by the reduction temperature. Indeed, even if a higher amount of Ni species was reduced with the increase of the pre-reduction temperature, sintering processes led to bigger Ni particles, and no impact on the catalytic performances was verified. Thus, data for the 14%Ni/USY zeolite pre-reduced at 470ºC can be directly compared to the obtained for the Mg-Ni/USY reduced at 700ºC. After pre-reduction of the Ni-Mg zeolites at higher temperature, it can be observed that the presence of Mg clearly leads to an important enhancement of the CO_2 conversion, as already previously found for the lower Ni content zeolites. Indeed, at 340ºC the CO_2 conversion raised from 35% on the 14%Ni/USY to 53% on the 9%Mg 13%Ni/USY. In addition, CH_4 selectivity was always higher than 92% on the Mg-Ni sample reduced at 700ºC. Besides the greater amount of reduced Ni species, the enhancement of the catalytic results after pre-reduction at 700ºC could be attributed to the prevention of the Ni particles sintering due to the presence of MgO on the sample, as already referred in the literature[9,10,15]. Finally, a commercial catalyst containing 10%Ni over γ-Al_2O_3 was tested and the results were included in Figure 12A. However, it is necessary to take into account that the density of the commercial catalyst is 850 $kg.m^{-3}$, while the density of the zeolite samples is always ~2200 $kg.m^{-3}$. As the mass of

catalyst was kept constant (same WHSV), this difference in the densities will affect the height of the catalyst bed, so that the comparison between the commercial and the zeolite samples is not straightforward. Moreover, even though this is not an optimized zeolite-based catalyst, conversions and selectivities are not significantly different from those obtained with the commercial catalyst.

In order to test the stability of a Mg-Ni/USY sample under reaction conditions at a fixed temperature in a long term test, the sample leading to the best catalytic results, 9%Mg 13%Ni/USY, was tested at 400ºC during 10h. In addition, a long term test was also performed for the commercial 10%Ni/ γ-Al_2O_3 at the same conditions. The results can be found in Figure 12B. Thus, it can be seen that both the conversion and the selectivity remain almost unchanged after the test whatever the catalyst (~3% of CO_2 conversion and ~1% of CH_4 selectivity losses in the Mg-Ni sample and ~2% of CO_2 conversion and ~1% of CH_4 selectivity losses in the commercial one). This clearly proves that the reported Mg-Ni/USY zeolite is promising in terms of stability, since the results after 10h under reaction conditions are comparable to those obtained for a commercial sample.

3.3.2. Mg as compensating cation

In addition, the two samples Mg-exchanged USY zeolites were also impregnated with 15%Ni. Concerning the XRD diffractograms (Figure 13A), the presence of Ni as NiO was found in all samples, as well as a small shift of the NiO peak (smaller than the observed for the samples with lower Ni content) was detected, indicating again that a fraction of Mg will not be present as compensating cation on these catalysts. According to the H_2-TPR profiles (Figure 13B), Mg leads to a more favoured reducibility of the Ni species, as observed by the shift towards lower temperatures of the maximum of the reduction peak. A decrease of the amount of Ni species strongly interacting with the support (T > 400ºC) could then be observed. New reduction peaks are also found as in the case of the ~5%Ni samples, indicating that also a fraction of Mg and Ni are present as mixed oxides, especially in the sample with higher Mg content.

Finally, the catalytic performances obtained for the Mg-exchanged samples containing 15% of Ni (Figure 14), when compared to the reference 15%Ni/H-USY, show that the Mg addition as compensating cation also benefits the catalytic performances, as previously observed for the samples presenting 5% of Ni. Nevertheless, in this case, better results were found when a smaller amount of Mg (0.7%) is exchanged. In fact, an increase of 40% in the

CO_2 conversion (350ºC) and 15% in the CH_4 selectivity (400ºC) can be obtained with this sample. At higher Mg content, the partial formation of Mg-Ni-O mixed oxides slightly decreases the reducibility of Ni species on this sample, which could lead to the observed not so good results.

4. Conclusions

The effect of the magnesium incorporation by incipient wetness impregnation and ion-exchange to Ni-based zeolites for the CO_2 methanation was studied. The impregnation of 0.9-2.5% of Mg on a 4.8%Ni/USY zeolite led to an important enhancement of the catalytic performances, with conversions up to 15% higher than that for the 4.8%Ni/USY being achieved. Indeed, Ni^0 particles with a considerably lower size than that calculated for the Ni/USY catalyst were formed through Mg addition. Moreover, the presence of higher amount of defective surfaces containing low-coordinated or protruded oxygen atoms at lower Mg contents could favour the CO_2 molecule activation. On the other hand, impregnation with Mg > 5.6% is responsible for the formation of NiO-MgO solid solutions, which decreases the crystallinity of the zeolite and the reducibility of the Ni species, decreasing the amount of Ni^0 active sites available for the H_2 dissociation. Consequently, no beneficial effects could be verified for the impregnation of Mg at higher contents.

Furthermore, it was observed that the presence of Mg as compensating cation in the zeolite support also enhances the activity of the catalysts for the CO_2 methanation. The improvements achieved could be attributed to the additional activation of the CO_2 molecules on Mg^{2+}, the more dispersed Ni particles, as well as to the higher Ni reducibility when compared to the Mg-impregnated due to the smaller formation of NiO-MgO solid solution.

The positive effect of adding Mg by impregnation and ion-exchange was also confirmed for samples containing higher Ni samples. The stability of the Mg-impregnated sample with higher Ni content was also tested in a long term test, and no relevant losses of CO_2 conversion and/or selectivity to CH_4 were observed.

Thus, it was proved that the Mg incorporation by impregnation or ion-exchange to Ni based zeolites can lead to beneficial effects on the catalytic performances for the CO_2 methanation.

Acknowledgment

M.C. Bacariza thanks to Fundação para a Ciência e Tecnologia (FCT) for her PhD grant (SFRK/BD/52369/2013) and for the financial support of the CQE research group (UID/QUI/00100/2013). The authors thank also to CEOPS Project (CO_2 - loop for Energy storage and conversion to Organic chemistry through advanced catalytic Processes Systems), which has received funds from the European Union's Seventh Framework Programme for research, technological development and demonstration under grant agreement number [309984].

References

(1) Aresta, M.; Dibenedetto, A. *Dalton Trans.* **2007**, No. 28, 2975.
(2) Aresta, M.; Dibenedetto, A.; Angelini, A. *J. CO2 Util.* **2013**, *3–4*, 65–73.
(3) Wei, W.; Jinlong, G. *Front. Chem. Sci. Eng.* **2011**, *5* (1), 2–10.
(4) Hoekman, S. K.; Broch, A.; Robbins, C.; Purcell, R. *Int. J. Greenh. Gas Control* **2010**, *4* (1), 44–50.
(5) Swapnesh, A.; Srivastava, V. C.; Mall, I. D. *Chem. Eng. Technol.* **2014**, *37* (10), 1765–1777.
(6) Wang, W.; Wang, S.; Ma, X.; Gong, J. *Chem. Soc. Rev.* **2011**, *40* (7), 3703–3727.
(7) Park, J.-N.; McFarland, E. W. *J. Catal.* **2009**, *266* (1), 92–97.
(8) Kim, H. Y.; Lee, H. M.; Park, J.-N. *J. Phys. Chem. C* **2010**, *114* (15), 7128–7131.
(9) Takezawa, N.; Terunuma, H.; Shimokawabe, M.; Kobayashib, H. *Appl. Catal.* **1986**, *23* (2), 291–298.
(10) Guo, M.; Lu, G. *Catal. Commun.* **2014**, *54*, 55–60.
(11) Fan, Z.; Sun, K.; Rui, N.; Zhao, B.; Liu, C. *J. Energy Chem.* **2015**, *24* (5), 655–659.
(12) Liu, J.; Cui, D.; Yu, J.; Su, F.; Xu, G. *Chin. J. Chem. Eng.* **2015**, *23* (1), 86–92.
(13) He, L.; Lin, Q.; Liu, Y.; Huang, Y. *J. Energy Chem.* **2014**, *23* (5), 587–592.
(14) Xu, L.; Wang, F.; Chen, M.; Yang, H.; Nie, D.; Qi, L.; Lian, X. *RSC Adv.* **2017**, *7* (30), 18199–18210.
(15) Tan, M.; Wang, X.; Wang, X.; Zou, X.; Ding, W.; Lu, X. *J. Catal.* **2015**, *329*, 151–166.
(16) Pirngruber, G. D.; Raybaud, P.; Belmabkhout, Y.; Čejka, J.; Zukal, A. *Phys. Chem. Chem. Phys.* **2010**, *12* (41), 13534–13546.
(17) Concepción-Heydorn, P.; Jia, C.; Herein, D.; Pfänder, N.; Karge, H. G.; Jentoft, F. C. *J. Mol. Catal. Chem.* **2000**, *162* (1–2), 227–246.
(18) Walton, K. S.; Abney, M. B.; Douglas LeVan, M. *Microporous Mesoporous Mater.* **2006**, *91* (1–3), 78–84.
(19) Barthomeuf∗, D. *Catal. Rev.* **1996**, *38* (4), 521–612.
(20) Yang, S.-T.; Kim, J.; Ahn, W.-S. *Microporous Mesoporous Mater.* **2010**, *135* (1–3), 90–94.
(21) Díaz, E.; Muñoz, E.; Vega, A.; Ordóñez, S. *Chemosphere* **2008**, *70* (8), 1375–1382.
(22) Coughlan, B.; Keane, M. A. *Zeolites* **1991**, *11* (1), 2–11.
(23) Graça, I.; González, L. V.; Bacariza, M. C.; Fernandes, A.; Henriques, C.; Lopes, J. M.; Ribeiro, M. F. *Appl. Catal. B Environ.* **2014**, *147*, 101–110.
(24) Bacariza, M. C.; Graça, I.; Westermann, A.; Ribeiro, M. F.; Lopes, J. M.; Henriques, C. *Top. Catal.*
(25) Westermann, A.; Azambre, B.; Bacariza, M. C.; Graça, I.; Ribeiro, M. F.; Lopes, J. M.; Henriques, C. *Appl. Catal. B Environ.* **2015**, *174–175*, 120–125.
(26) Aziz, M. a. A.; Jalil, A. A.; Triwahyono, S.; Ahmad, A. *Green Chem.* **2015**, *17* (5), 2647–2663.
(27) Hu, D.; Gao, J.; Ping, Y.; Jia, L.; Gunawan, P.; Zhong, Z.; Xu, G.; Gu, F.; Su, F. *Ind. Eng. Chem. Res.* **2012**, *51* (13), 4875–4886.
(28) Ruckenstein, E.; Hang Hu, Y. *Appl. Catal. Gen.* **1999**, *183* (1), 85–92.
(29) Meshkani, F.; Rezaei, M. *Catal. Commun.* **2011**, *12* (11), 1046–1050.
(30) Meshkani, F.; Rezaei, M. *J. Nat. Gas Chem.* **2011**, *20* (2), 198–203.
(31) Kong, M.; Yang, Q.; Fei, J.; Zheng, X. *Int. J. Hydrog. Energy* **2012**, *37* (18), 13355–13364.

(32) Kwak, B. S.; Lee, J. S.; Lee, J. S.; Choi, B.-H.; Ji, M. J.; Kang, M. *Appl. Energy* **2011**, *88* (12), 4366–4375.
(33) Abdollahifar, M.; Haghighi, M.; Babaluo, A. A. *J. Ind. Eng. Chem.* **2014**, *20* (4), 1845–1851.
(34) Guo, J.; Lou, H.; Zhao, H.; Chai, D.; Zheng, X. *Appl. Catal. Gen.* **2004**, *273* (1–2), 75–82.
(35) Shou-Yong, J.; Li-Bin, L.; Ning-Kang, H.; Jin, Z.; Yong, L. *J. Mater. Sci. Lett.* **2000**, *19* (3), 225–227.
(36) Yang, W.; Feng, Y.; Chu, W. *J. Nanotechnol.* **2014**, *2014*, e547030.
(37) Guo, J.; Lou, H.; Zhao, H.; Zheng, X. *React. Kinet. Catal. Lett.* **2005**, *84* (1), 93–100.
(38) Kawabata, T.; Shinozuka, Y.; Ohishi, Y.; Shishido, T.; Takaki, K.; Takehira, K. *J. Mol. Catal. Chem.* **2005**, *236* (1–2), 206–215.
(39) Choudhary, V. R.; Uphade, B. S.; Mamman, A. S. *J. Catal.* **1997**, *172* (2), 281–293.
(40) Parmaliana, A.; Arena, F.; Frusteri, F.; Giordano, N. *J. Chem. Soc. Faraday Trans.* **1990**, *86* (14), 2663–2669.
(41) *Oxide Surfaces*; Elsevier, 2001.
(42) Zhang, J.; Singh, R.; Webley, P. A. *Microporous Mesoporous Mater.* **2008**, *111* (1–3), 478–487.
(43) Graça, I.; Iruretagoyena, D.; Chadwick, D. *Appl. Catal. B Environ.* **2017**, *206*, 434–443.

Table captions

Table 1 - Physicochemical and textural properties of the commercial HNaUSY zeolite.

Table 2 - Preparation conditions and associated labels for the several prepared catalysts.

Table 3 - Textural properties of Ni samples with Mg impregnated and as compensating cation and reference zeolite.

Table 4 - Relationship between the Ni/(Ni+Mg) in samples with low Ni content analysed in this study and corresponding catalytic performances.

Table 1:

Unit cell formula	Si/Al [a]	Si/Al_{IV} [b]	EFAL	V_{micro} (cm^3g^{-1})	V_{meso} (cm^3g^{-1})	S_{ext} (m^2g^{-1})
$Na_{17}H_{21}Al_{39}Si_{153}O_{384}$	2.8	4.0	16	0.299	0.032	13

V_{micro} = micropore volume; V_{meso} = mesopore volume; S_{ext} = external surface area

[a] Global Si/Al ratio determined from elemental analysis.

[b] Framework Si/Al ratio calculated from the unit cell parameter (a_0= 2.535 nm), using the Breck-Flanigen equation.

EFAL**:** extra-framework aluminium species.

Table 2:

	Label	Observations
Reference catalysts	**MgO**	Commercial MgO from Merck.
	NiO	Commercial NiO from Sigma Aldrich.
	7.0%Mg/USY	7.0%Mg over USY zeolite prepared by incipient wetness impregnation. Calcination at 500ºC under air flow.
	5.0%Ni/MgO	5%Ni over commercial MgO prepared by incipient wetness impregnation. Calcination at 500ºC under air flow.
Study 1. Mg incorporated by impregnation	**4.8%Ni/USY** **14%Ni/USY**	4.8%Ni and 14%Ni respectively over USY zeolite prepared by incipient wetness preparation. Calcination at 500ºC under air flow.
	0.9%Mg 4.3%Ni/USY **2.5%Mg 3.7%Ni/USY** **5.6%Mg 4.3%Ni/USY** **13.0%Mg 3.5%Ni/USY**	Impregnation of different %Mg over 4.8%Ni/USY. Calcination at 500ºC under air flow.
	9%Mg 13%Ni/USY	Impregnation of Mg over 14%Ni/USY. Calcination at 500ºC under air flow.
Study 2. Mg incorporated by ion-exchange	**4.8%Ni/H-USY** **15%Ni/H-USY**	4.8%Ni and 14%Ni respectively over H-USY zeolite prepared as shown on Figure 1. Ni was incorporated by incipient wetness impregnation. Calcination at 500ºC under air flow.
	4.3%Ni/0.7%Mg-USY$_{IE}$ **4.5%Ni/1.4%Mg-USY$_{IE}$** **15%Ni/0.7%Mg-USY$_{IE}$** **15%Ni/1.4%Mg-USY$_{IE}$**	Ion-exchange of USY zeolite with $Mg(NO_3)_2$ followed by incorporation of Ni by incipient wetness impregnation. Calcination after ion-exchange (100ºC) and impregnation (500ºC) under air flow.

Table 3:

Label	V_{micro} (cm^3/g)	V_{meso} (cm^3/g)	S_{ext} (cm^3/g)
USY	0.299	0.032	13
4.8%Ni/USY	0.297	0.019	10
2.5%Mg 3.7%Ni/USY	0.295	0.022	13
13.0%Mg 3.5%Ni/USY	0.067	0.025	14
H-USY	0.295	0.066	37
4.3%Ni/0.7%MgUSY$_{IE}$	0.324	0.055	21
4.5%Ni/1.4%MgUSY$_{IE}$	0.311	0.060	28

Table 4:

Ni/(Ni+Mg)	CO_2 conversion (%)	CH_4 Selecitivity (%)
1.0	23	62
0.8	28	68
0.6	39	74
0.4	33	64
0.2	24	51
0.0	3	0

Figure captions

Figure 1 - Ion-exchange procedure for Mg exchanged samples.

Figure 2 - Powder XRD diffractograms of the parent USY zeolite (a); 4.8%Ni/USY (b); 0.9%Mg 4.3%Ni/USY (c); 2.5%Mg 3.7%Ni/USY (d); 5.6%Mg 4.3%Ni/USY (e) and 13.0%Mg 3.5%Ni/USY from 5 to 80ºC and the detailed diffractograms from 41.5 to 45.5º.

Figure 3 - H_2-TPR profiles of samples MgO (a); 7.0%Mg/USY (b); NiO (c); 4.8%Ni/USY (d); 5.0%Ni/MgO (e); 0.9%Mg 4.3%Ni/USY (f); 2.5%Mg 3.7%Ni/USY (g); 5.6%Mg 4.3%Ni/USY (h) and 13.0%Mg 3.5%Ni/USY (i).

Figure 4 - TEM micrographs for samples 4.8%Ni/USY (A); 0.9%Mg 4.3%Ni/USY (B); 2.5%Mg 3.7%Ni/USY (C) and 13.0%Mg 3.5%Ni/USY (D).

Figure 5 - CO_2-TPD of samples USY, 4.8%Ni/USY and 2.5%Mg 3.7%Ni/USY.

Figure 6 - Catalytic performances of samples 4.8%Ni/USY (**A**,**B**,■); 4.8%Ni/MgO (**A**,**B**,□); 0.9%Mg 4.3%Ni/USY (**A**,*); 2.5%Mg 3.7%Ni/USY (**A**,●); 5.6%Mg 4.3%Ni/USY (**B**,O) and 13.0%Mg 3.5%Ni/USY (**B**,Δ).

Figure 7 - Powder XRD diffractograms of the parent USY zeolite (a); 4.8%Ni/USY (b); 4.3%Ni/0.7%Mg-USY_{IE} (c); 4.5%Ni/1.4%Mg-USY_{IE} (d) from 5 to 80ºC and the detailed diffractograms from 41.5 to 45.5º.

Figure 8 - H_2-TPR profiles obtained for samples 4.8%Ni/USY (a); 4.3%Ni/0.7%Mg-USY_{IE} (b) and 4.5%Ni/1.4%Mg-USY_{IE} (c).

Figure 9 - TEM micrographs for samples 4.8%Ni/USY (A); 4.3%Ni/0.7%Mg-USY_{IE} (B) and 4.5%Ni/1.4%Mg-USY_{IE} (C).

Figure 10 – (A) Catalytic performances of samples 4.8%Ni/H-USY (■); 4.3%Ni/0.7%Mg-USY_{IE} (▲) and 4.5%Ni/1.4%Mg-USY_{IE} (O); (B) CO_2-TPD profiles obtained for samples 2.5%Mg 3.7%Ni/USY and 4.5%Ni/1.4%Mg-USY_{IE}.

Figure 11 – Powder XRD diffractograms from 5 to 80ºC and detailed (41.5 to 45.5º) (A) and H_2-TPR profiles (B) obtained for samples 14%Ni/USY and 9%Mg 13%Ni/USY.

Figure 12 – (A) Catalytic performances of samples 14%Ni/USY (■); 9%Mg 13%Ni/USY reduced at 470ºC (▲), 9%Mg 13%Ni/USY reduced at 700ºC (O) and a commercial 10%Ni/γ-Al_2O_3 catalyst (◊). 14%Ni/USY catalyst did not presented differences when increasing the pre-reduction temperature [24]. Thermodynamics are presented in dashed lines; (B) Long term test results obtained for 9%Mg 13%Ni/USY reduced at 700ºC (O) and the commercial 10%Ni/γ-Al_2O_3 (♦) during 10h at 400ºC under reaction conditions.

Figure 13 – Powder XRD diffractograms from 5 to 80ºC and detailed (41.5 to 45.5º) (A) and H_2-TPR profiles (B) obtained for samples 15%Ni/H-USY, 15%Ni/0.7%Mg-USY_{IE} and 15%Ni/1.4%Mg-USY_{IE}.

Figure 14 - Catalytic performances of samples 15%Ni/H-USY (■); 15%Ni/0.7%Mg-USY_{IE} (▲) and 15%Ni/1.4%Mg-USY_{IE} (O). Thermodynamics are presented in dashed lines.

Figure 1:

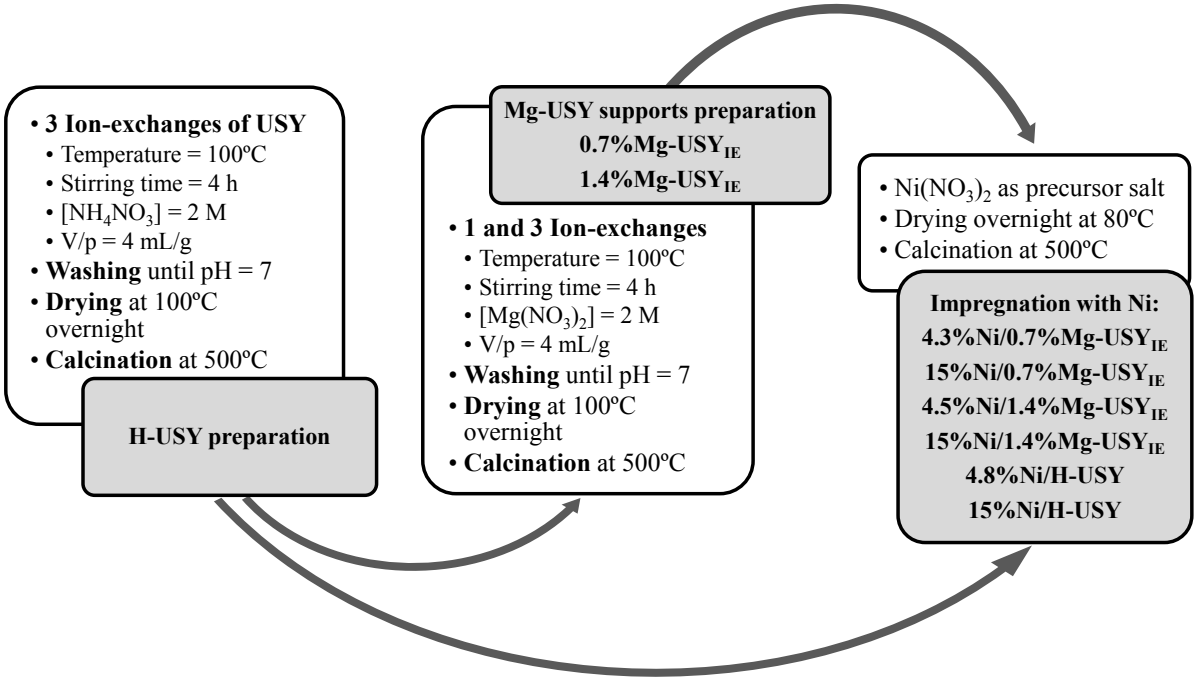
• 3 Ion-exchanges of USY
• Temperature = 100ºC
• Stirring time = 4 h
• [NH4NO3] = 2 M
• V/p = 4 mL/g
• Washing until pH = 7
• Drying at 100ºC overnight
• Calcination at 500ºC
H-USY preparation
Mg-USY supports preparation
0.7%Mg-USYIE
1.4%Mg-USYIE
• 1 and 3 Ion-exchanges
• Temperature = 100ºC
• Stirring time = 4 h
• [Mg(NO3)2] = 2 M
• V/p = 4 mL/g
• Washing until pH = 7
• Drying at 100ºC overnight
• Calcination at 500ºC
• Ni(NO3)2 as precursor salt
• Drying overnight at 80ºC
• Calcination at 500ºC
Impregnation with Ni:
4.3%Ni/0.7%Mg-USYIE
15%Ni/0.7%Mg-USYIE
4.5%Ni/1.4%Mg-USYIE
15%Ni/1.4%Mg-USYIE
4.8%Ni/H-USY
15%Ni/H-USY

Figure 2:

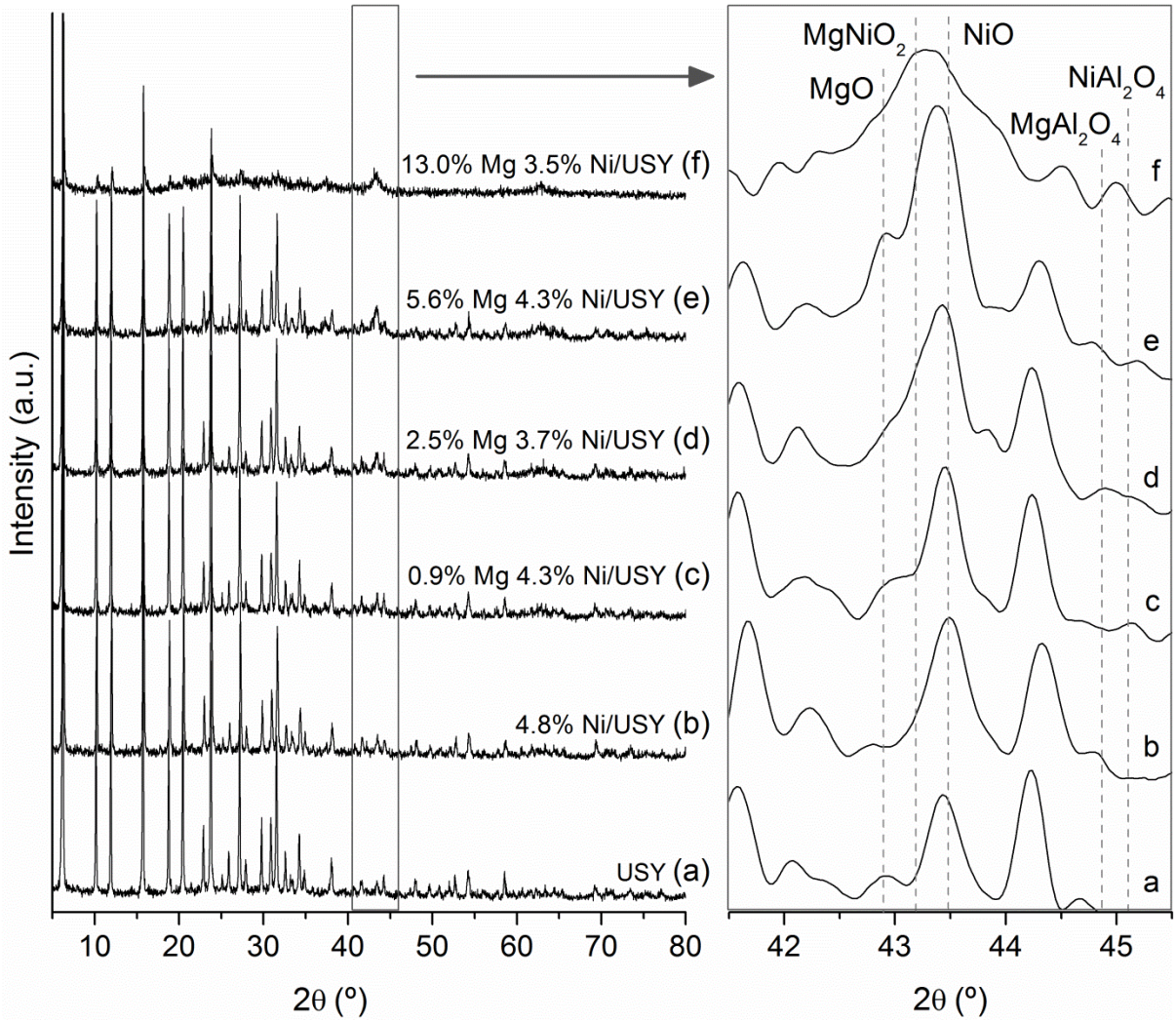
Intensity (a.u.)
13.0% Mg 3.5% Ni/USY (f)
5.6% Mg 4.3% Ni/USY (e)
2.5% Mg 3.7% Ni/USY (d)
0.9% Mg 4.3% Ni/USY (c)
4.8% Ni/USY (b)
USY (a)
10
20
30
40
50
60
70
80
2θ (°)
MgNiO2
NiO
MgO
NiAl2O4
MgAl2O4
f
e
d
c
b
a
42
43
44
45
2θ (°)

Figure 3:

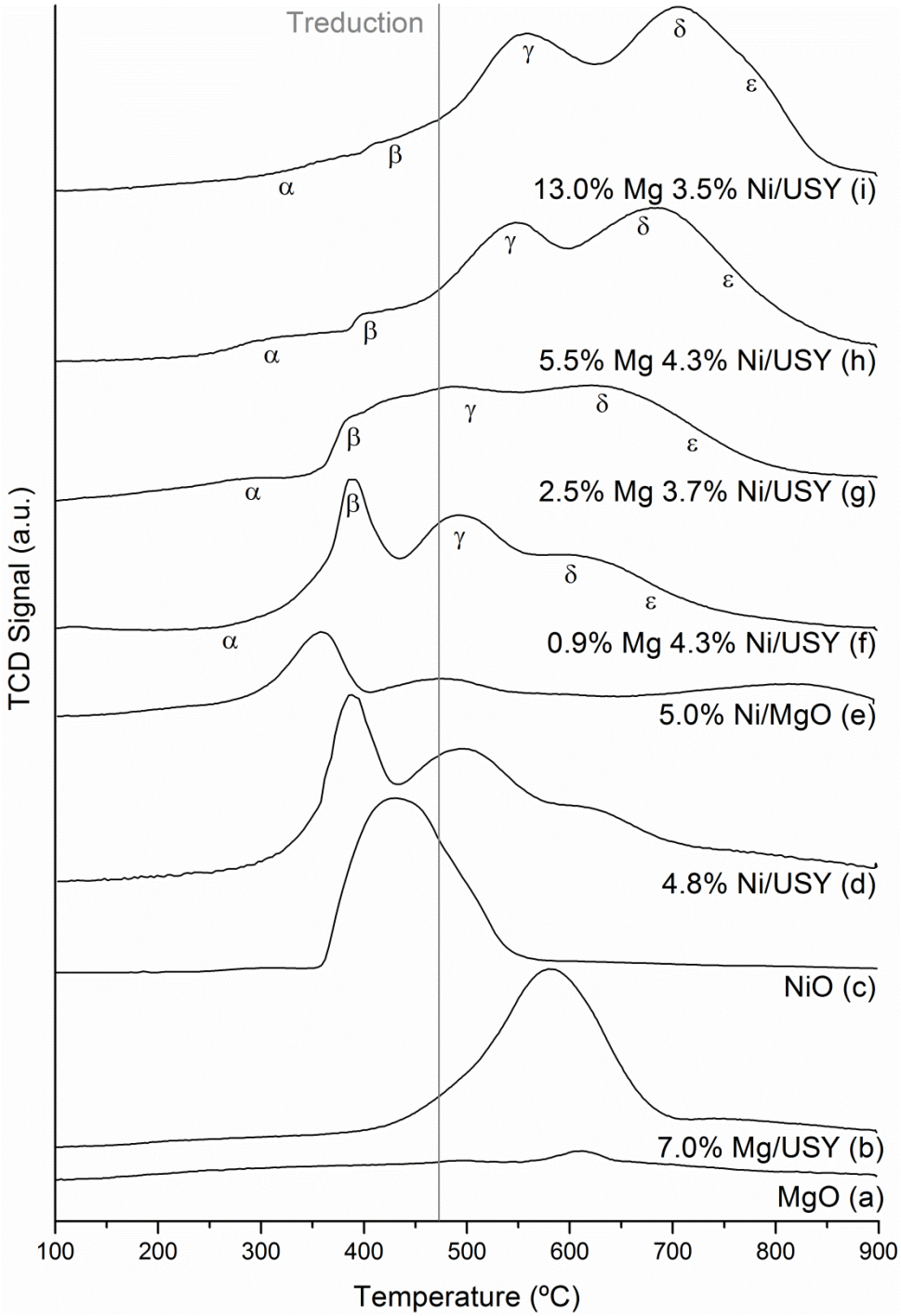
Treduction
α
β
γ
δ
ε
13.0% Mg 3.5% Ni/USY (i)
5.5% Mg 4.3% Ni/USY (h)
2.5% Mg 3.7% Ni/USY (g)
0.9% Mg 4.3% Ni/USY (f)
5.0% Ni/MgO (e)
4.8% Ni/USY (d)
NiO (c)
7.0% Mg/USY (b)
MgO (a)
TCD Signal (a.u.)
100
200
300
400
500
600
700
800
900
Temperature (ºC)

Figure 4:

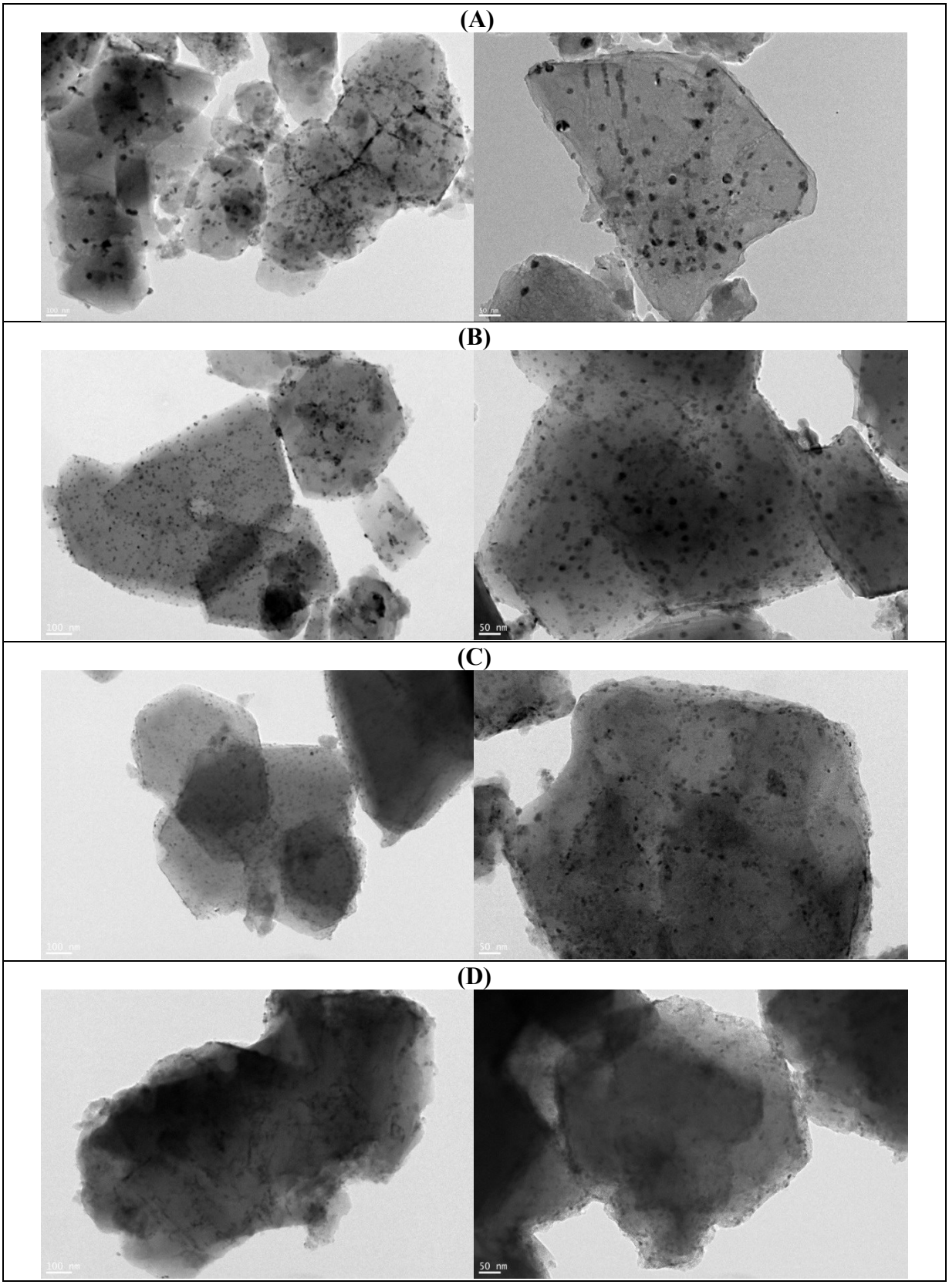

Figure 5:

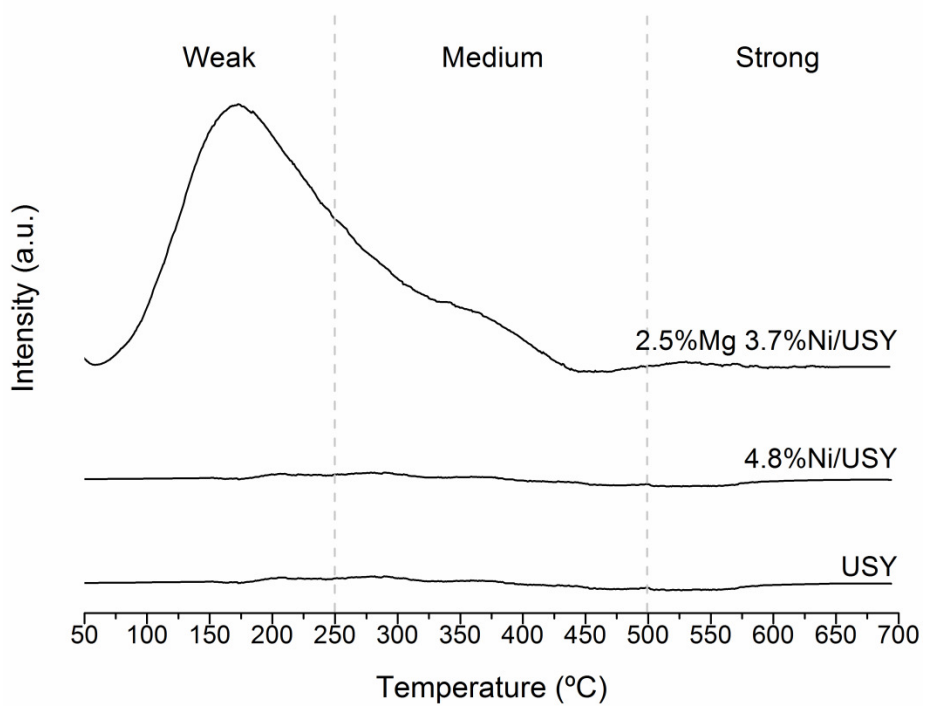
Weak
Medium
Strong
Intensity (a.u.)
2.5%Mg 3.7%Ni/USY
4.8%Ni/USY
USY
50 100 150 200 250 300 350 400 450 500 550 600 650 700
Temperature (°C)

Figure 6:

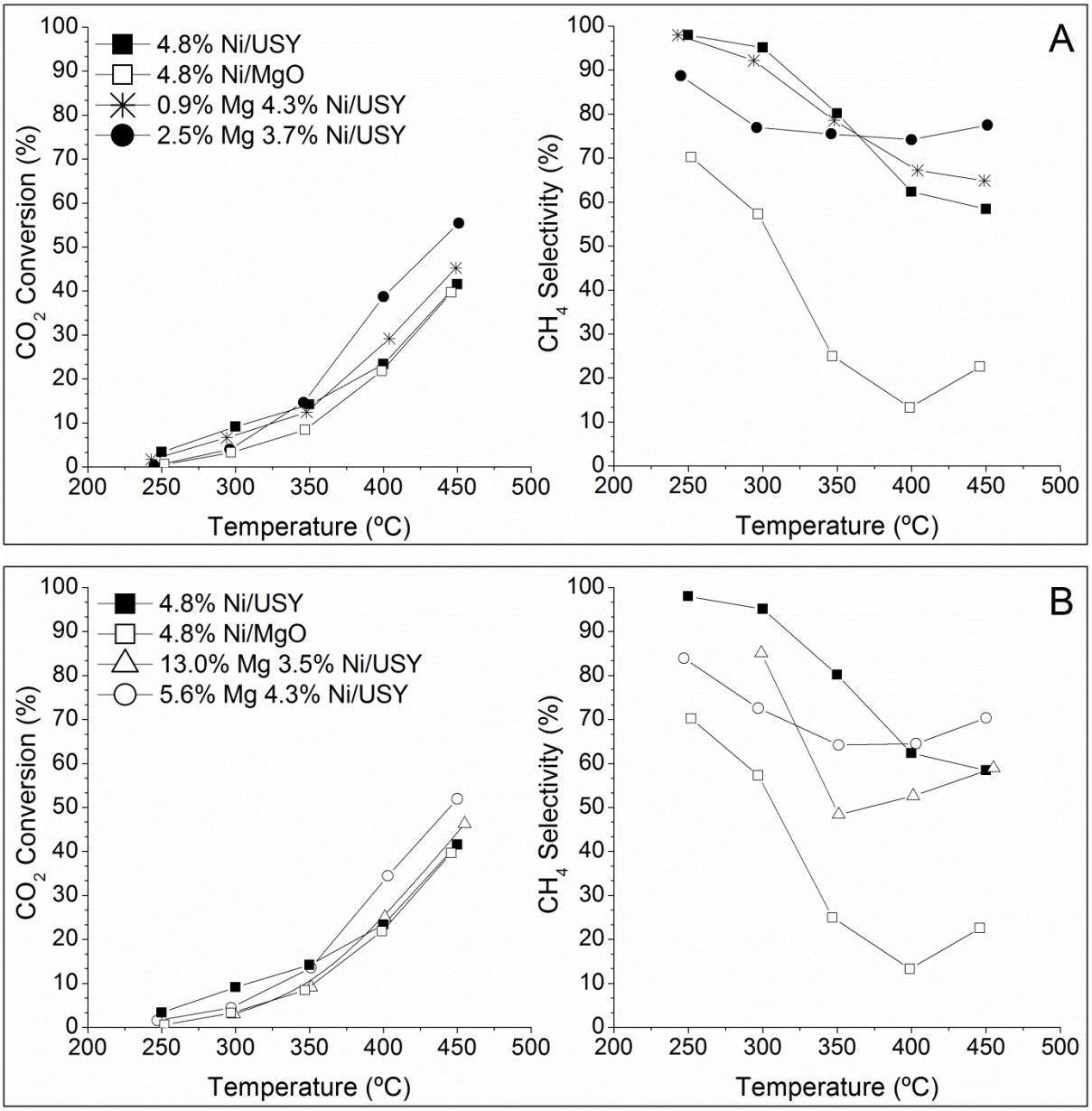
A
4.8% Ni/USY
4.8% Ni/MgO
0.9% Mg 4.3% Ni/USY
2.5% Mg 3.7% Ni/USY
CO2 Conversion (%)
CH4 Selectivity (%)
Temperature (ºC)
Temperature (ºC)
B
4.8% Ni/USY
4.8% Ni/MgO
13.0% Mg 3.5% Ni/USY
5.6% Mg 4.3% Ni/USY
CO2 Conversion (%)
CH4 Selectivity (%)
Temperature (ºC)
Temperature (ºC)

Figure 7:

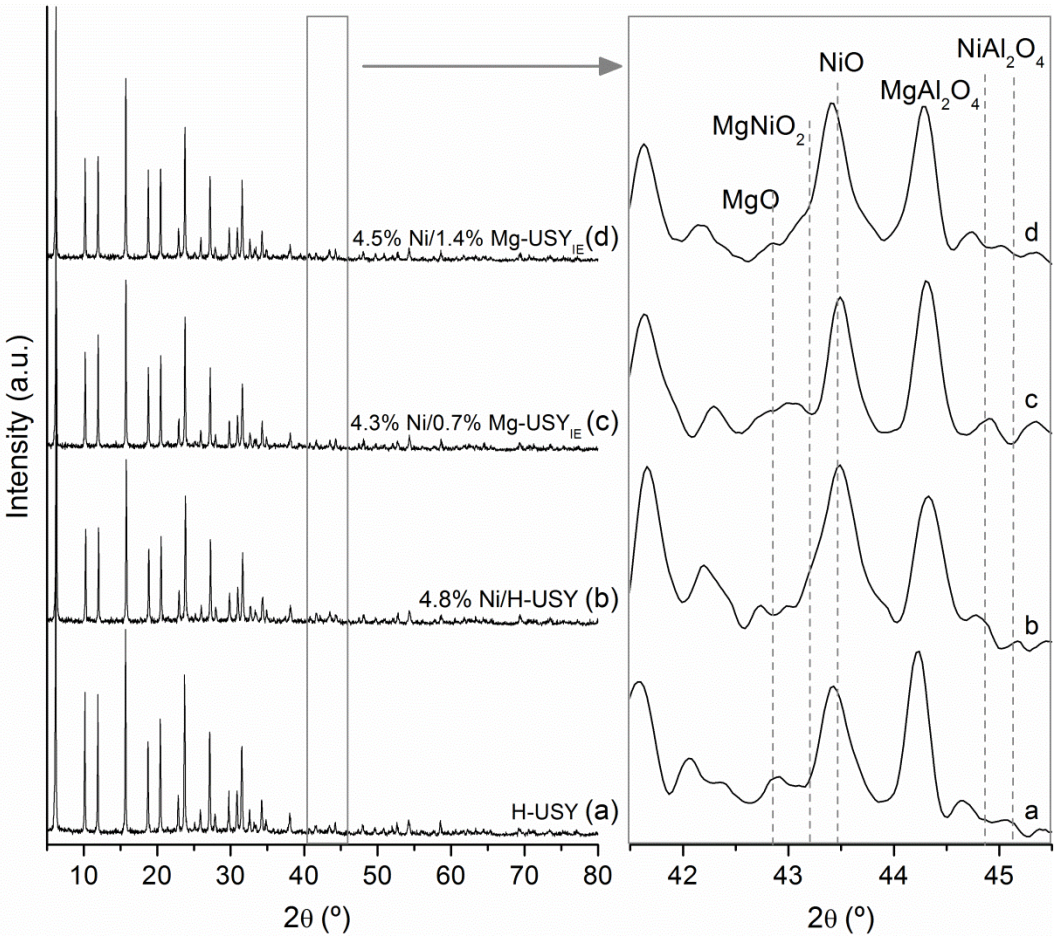
Intensity (a.u.)
4.5% Ni/1.4% Mg-USY$_{IE}$ (d)
4.3% Ni/0.7% Mg-USY$_{IE}$ (c)
4.8% Ni/H-USY (b)
H-USY (a)
10
20
30
40
50
60
70
80
2θ (°)
MgO
MgNiO$_2$
NiO
MgAl$_2$O$_4$
NiAl$_2$O$_4$
d
c
b
a
42
43
44
45
2θ (°)

Figure 8:

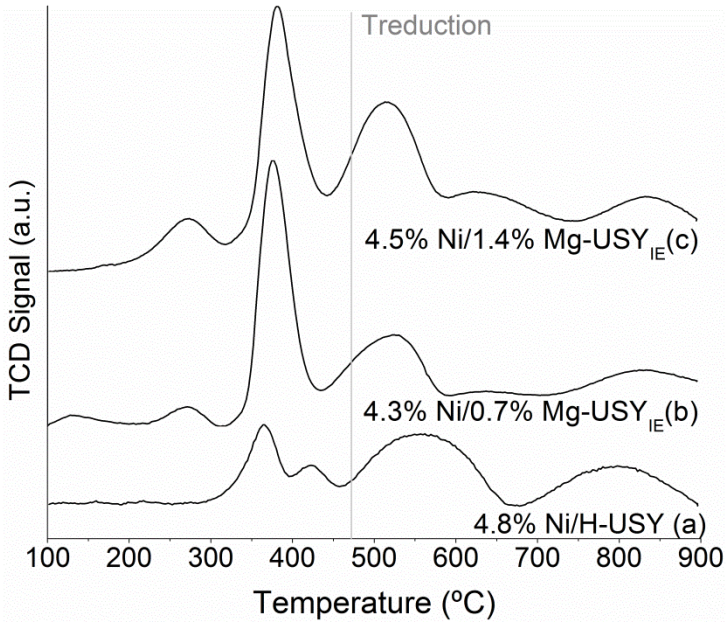
Treduction
4.5% Ni/1.4% Mg-USY$_{IE}$(c)
4.3% Ni/0.7% Mg-USY$_{IE}$(b)
4.8% Ni/H-USY (a)
TCD Signal (a.u.)
100
200
300
400
500
600
700
800
900
Temperature (ºC)

Figure 9:

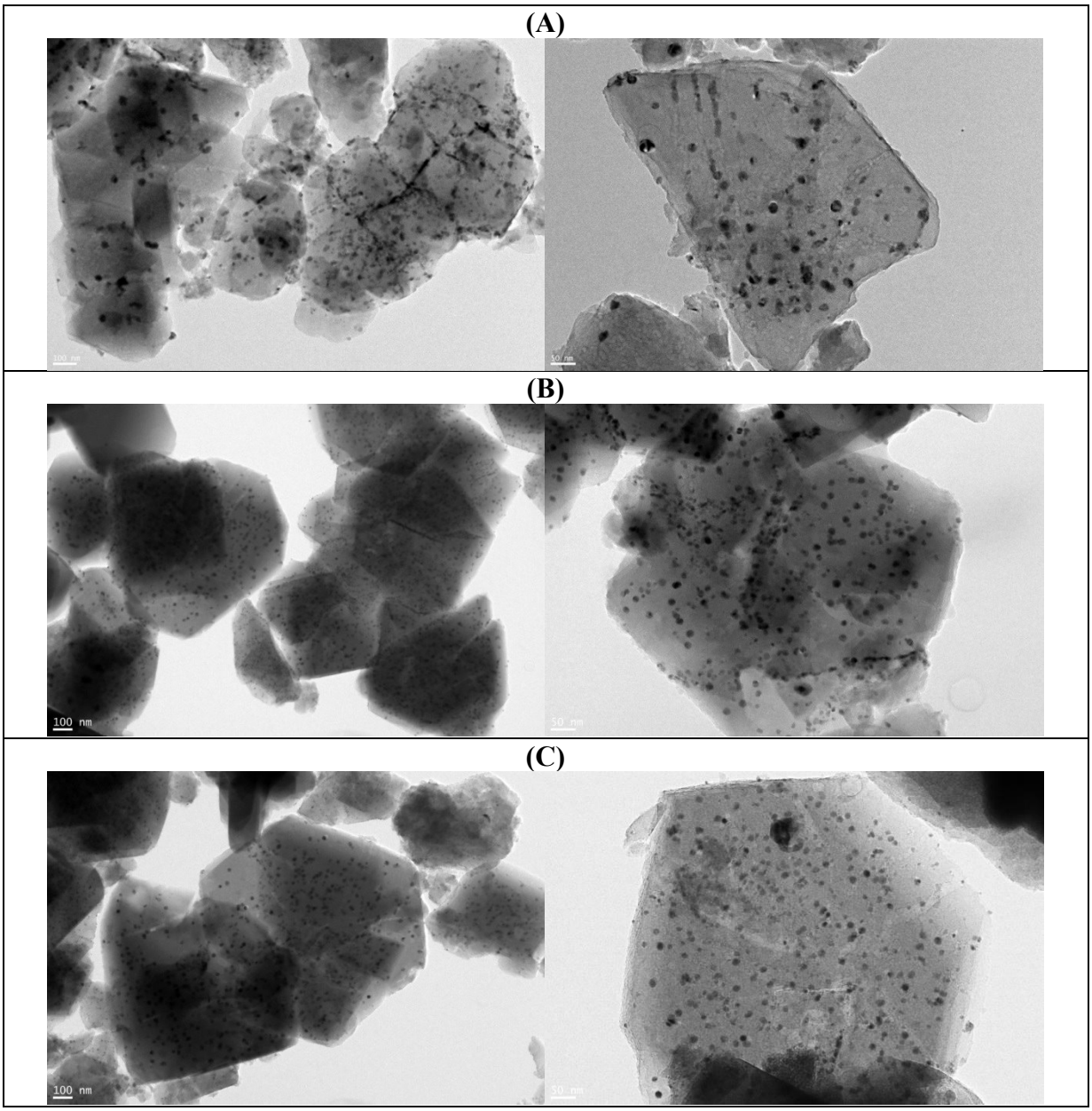

Figure 10:

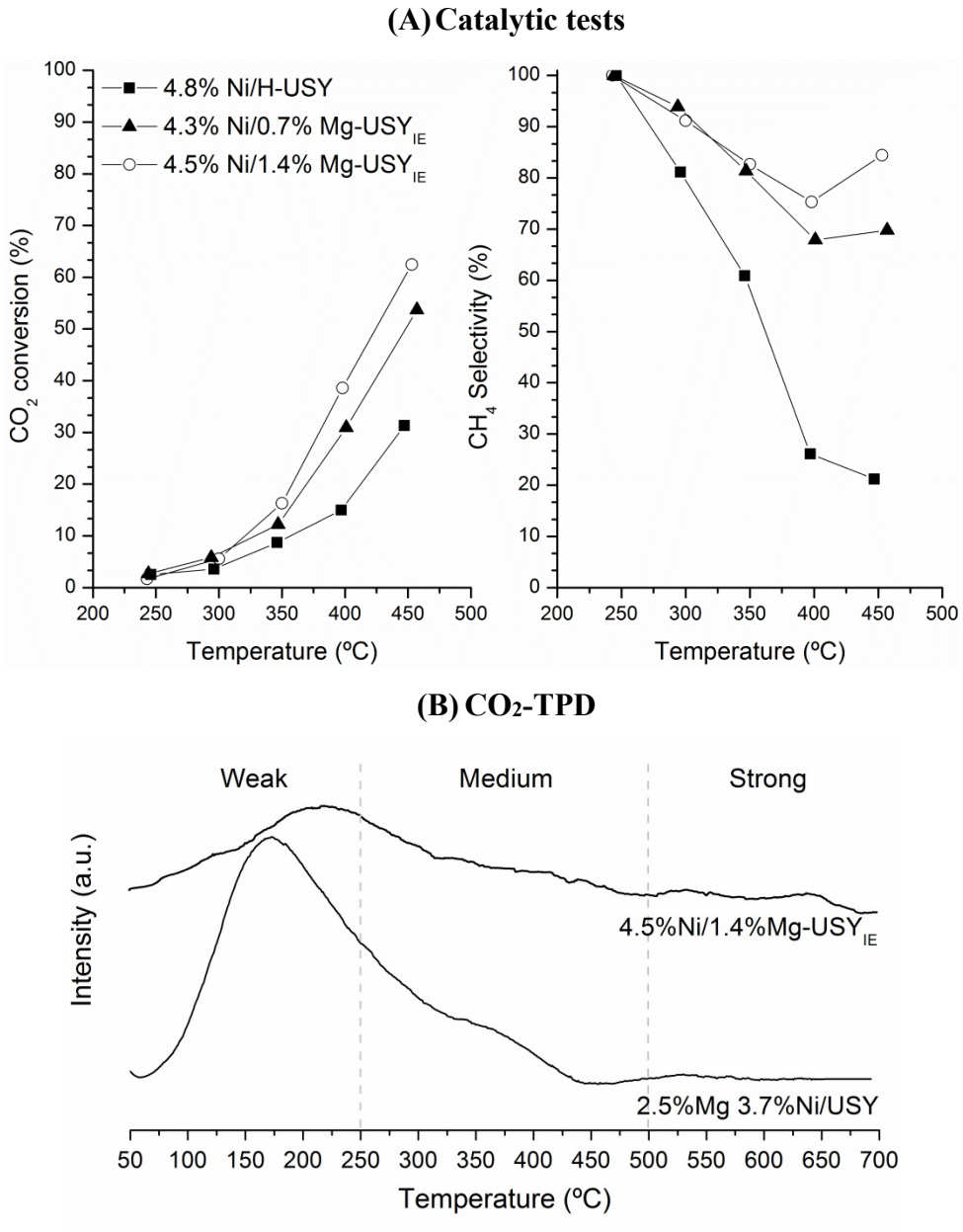
(A) Catalytic tests
4.8% Ni/H-USY
4.3% Ni/0.7% Mg-USY IE
4.5% Ni/1.4% Mg-USY IE
CO2 conversion (%)
CH4 Selectivity (%)
Temperature (ºC)
Temperature (ºC)
(B) CO2-TPD
Weak
Medium
Strong
Intensity (a.u.)
4.5%Ni/1.4%Mg-USY IE
2.5%Mg 3.7%Ni/USY
Temperature (ºC)

Figure 11

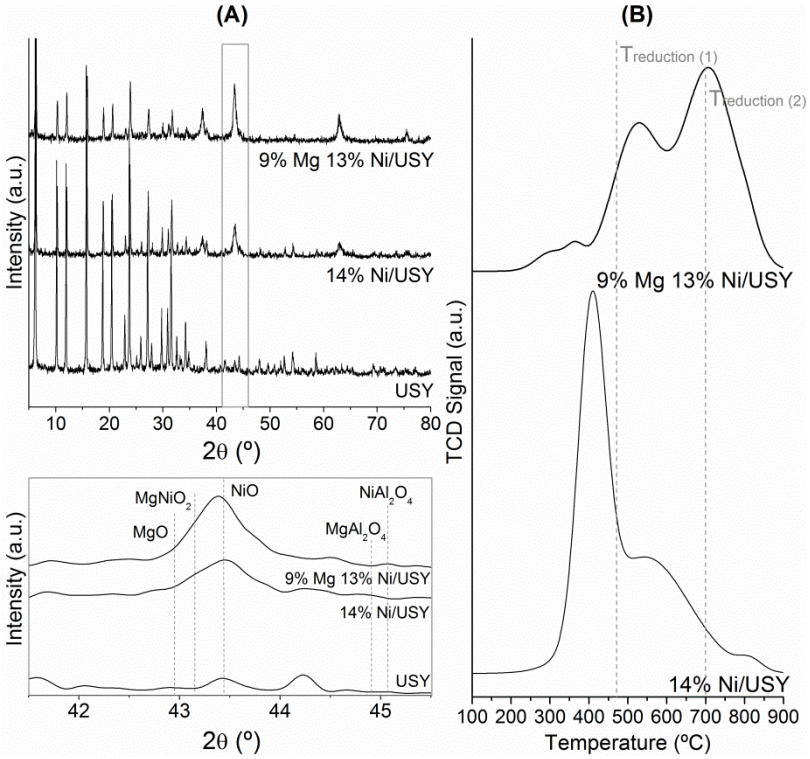
(A)
(B)
9% Mg 13% Ni/USY
14% Ni/USY
USY
Intensity (a.u.)
2θ (º)
MgNiO2
NiO
NiAl2O4
MgO
MgAl2O4
Treduction (1)
Treduction (2)
TCD Signal (a.u.)
Temperature (ºC)

Figure 12

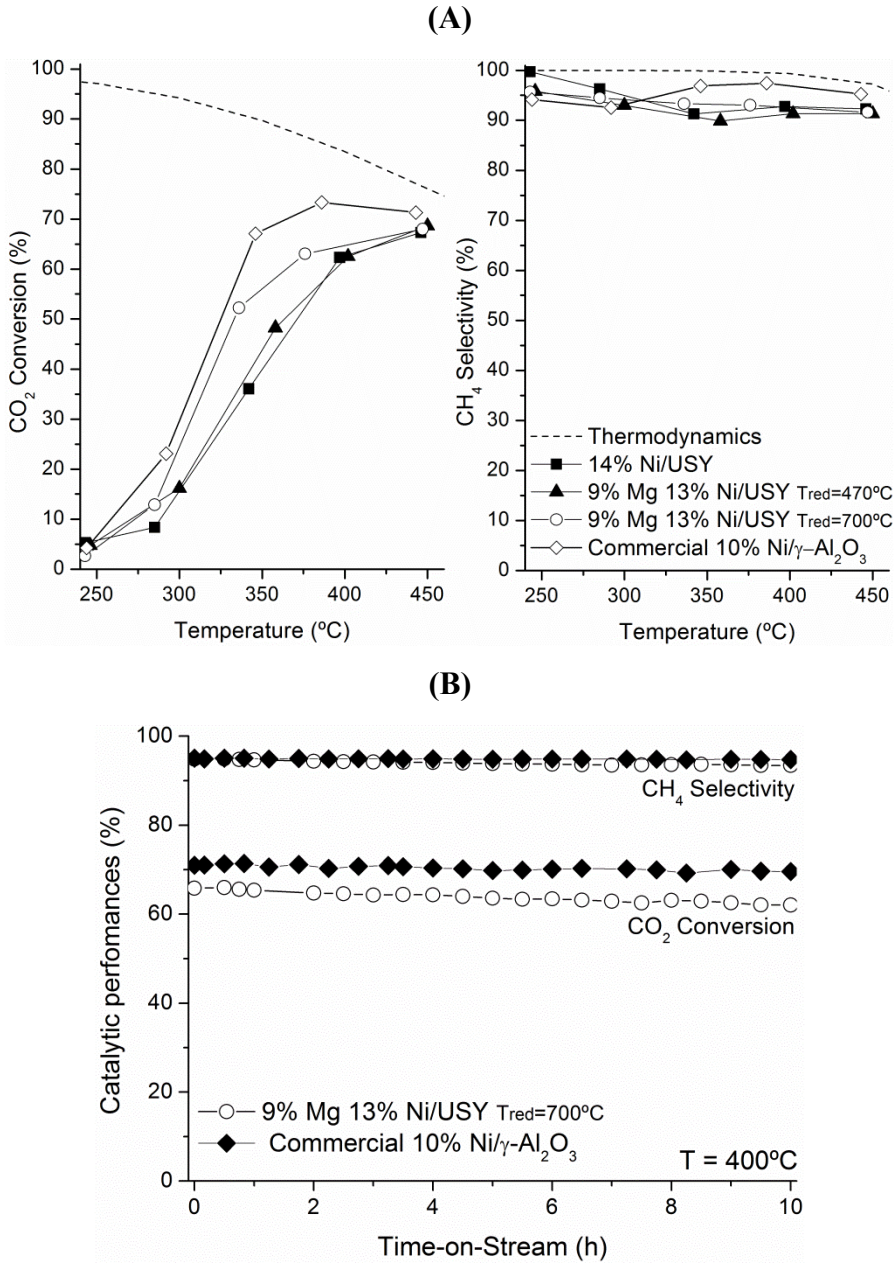
(A)
CO2 Conversion (%)
Temperature (ºC)
CH4 Selectivity (%)
Temperature (ºC)
Thermodynamics
14% Ni/USY
9% Mg 13% Ni/USY Tred=470ºC
9% Mg 13% Ni/USY Tred=700ºC
Commercial 10% Ni/γ–Al2O3
(B)
Catalytic perfomances (%)
CH4 Selectivity
CO2 Conversion
9% Mg 13% Ni/USY Tred=700ºC
Commercial 10% Ni/γ-Al2O3
T = 400ºC
Time-on-Stream (h)

Figure 13

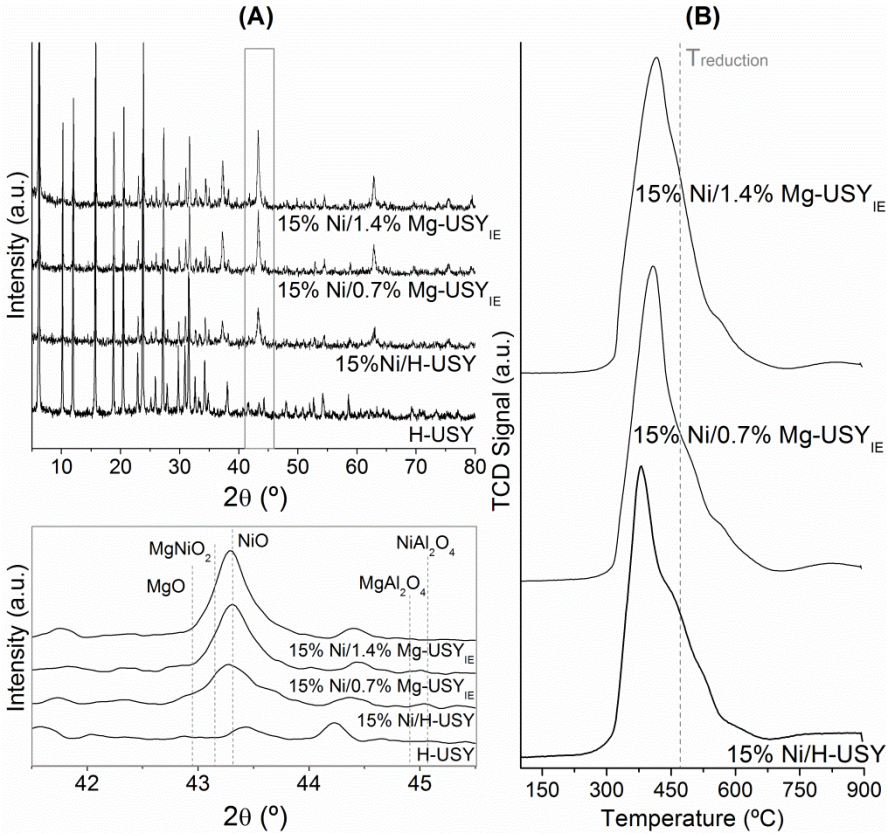
(A)
(B)
Intensity (a.u.)
15% Ni/1.4% Mg-USY$_{IE}$
15% Ni/0.7% Mg-USY$_{IE}$
15%Ni/H-USY
H-USY
10 20 30 40 50 60 70 80
2θ (º)
MgNiO$_2$
NiO
NiAl$_2$O$_4$
MgO
MgAl$_2$O$_4$
15% Ni/1.4% Mg-USY$_{IE}$
15% Ni/0.7% Mg-USY$_{IE}$
15% Ni/H-USY
H-USY
42 43 44 45
2θ (º)
T$_{reduction}$
TCD Signal (a.u.)
15% Ni/1.4% Mg-USY$_{IE}$
15% Ni/0.7% Mg-USY$_{IE}$
15% Ni/H-USY
150 300 450 600 750 900
Temperature (ºC)

Figure 14

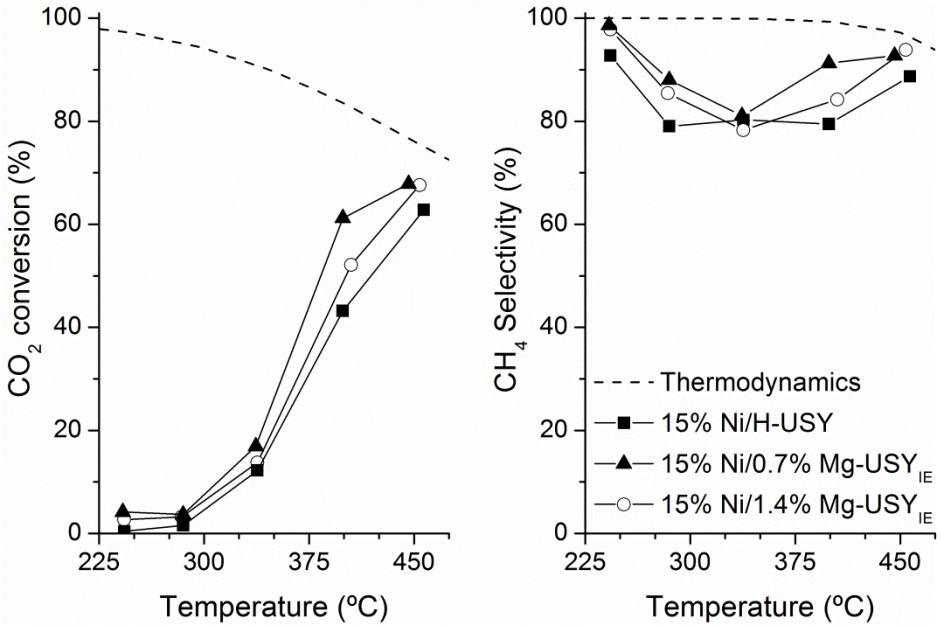
100
80
60
40
20
0
225
300
375
450
Temperature (ºC)
CO2 conversion (%)
CH4 Selectivity (%)
Thermodynamics
15% Ni/H-USY
15% Ni/0.7% Mg-USYIE
15% Ni/1.4% Mg-USYIE